HHS Public Access

Author manuscript

Cancer Lett. Author manuscript; available in PMC 2019 September 28.

Published in final edited form as:

Cancer Lett. 2018 September 28; 432: 169–179. doi:10.1016/j.canlet.2018.06.006.

Targeting Orai1-mediated store-operated calcium entry by RP4010 for anti-tumor activity in esophagus squamous cell carcinoma

Chaochu Cui[1,2,¶], **Yan Chang**[2,¶], **Xiaoli Zhang**[3], **Sangyong Choi**[2], **Henry Tran**[6], **Kumar V. Penmetsa**[4], **Srikant Viswanadha**[5], **Liwu Fu**[1,*], and **Zui Pan**[2,*]

[1]State Key Laboratory of Oncology in South China; Collaborative Innovation Center for Cancer Medicine, Sun Yat-sen University Cancer Center, Guangzhou, China [2]College of Nursing and Health Innovation, University of Texas at Arlington, Arlington, TX, USA [3]Comprehensive Cancer Center, The Ohio State University Medical Center, Columbus, OH, USA [4]Rhizen Pharmaceuticals SA, La Chaux-de-Fonds, Switzerland [5]Incozen Therapeutics Private Limited, Hyderabad, India [6]Department of Biology, University of Texas at Arlington, Arlington, TX, USA

Abstract

Esophageal cancer (EC) is the 6th leading cause of cancer mortality worldwide with poor prognosis, hence more effective chemotherapeutic drugs for this deadly disease are urgently needed. We previously reported that high expression of Orai1, a store-operated Ca^{2+} entry (SOCE) channel was associated with poor survival rate in EC patients and Orai1-mediated intracellular Ca^{2+} oscillations regulated cancer cell proliferation. Previous studies suggested that Orai1-mediated SOCE is a promising target for EC chemotherapy. Here, we evaluated the anti-cancer effect of a novel SOCE inhibitor, RP4010, in cultured EC cells and xenograft models. Compared to other previously reported SOCE channel inhibitors, RP4010 is more potent in blocking SOCE and inhibiting cell proliferation in EC and other cancer cells. Treatment with RP4010 resulted in reduction of intracellular Ca^{2+} oscillations, caused cell cycle arrest at G0/G1 phase *in vitro,*

[*]Corresponding author: Zui Pan, Address: College of Nursing and Health Innovation, University of Texas at Arlington, 501 S. Nedderman Dr., Arlington, TX, USA, Telephone: +1-817-272-2595, zui.pan@uta.edu, Corresponding author: Liwu Fu, Address: State Key Laboratory of Oncology in South China, Collaborative Innovation Center for Cancer Medicine, Sun Yat-sen University Cancer Center, 651 E. Dongfeng St., Guangzhou, China, Telephone: +86-20-8734-3163, fulw@mail.sysu.edu.cn.
[¶]These authors contributed equally.

Authorship Contributions

Participated in research design: Zui Pan, Chaochu Cui, Yan Chang
Conducted experiments: Chaochu Cui, Yan Chang, Sangyong Choi, Henry Tran.
Performed data analysis: Chaochu Cui, Yan Chang, Xiaoli Zhang, Kumar V. Penmetsa, Srikant Viswanadha, Zui Pan.
Wrote or contributed to the writing of the manuscript: Chaochu Cui, Yan Chang, Liwu Fu, Zui Pan, Srikant Viswanadha, Kumar V. Penmetsa

Conflicts of interest

CC, YC, XZ, SC, HT, LF and ZP declare no conflict of interest. KVP is employed at Rhizen Pharmaceuticals SA and SV is employed at Incozen Therapeutics Private Limited. Rhizen and Incozen have a commercial interest in development of RP4010 as a lead compound.

decreased nuclear translocation of nuclear factor kappa B (NF-κB) *in vivo* and *in vitro*, and inhibited tumor growth *in vivo*. Taken together, data demonstrated the therapeutic potential of RP4010 in EC patients *via* inhibition of SOCE-mediated intracellular Ca^{2+} signaling.

Introduction

Esophageal cancer (EC) is the 6th leading cause of cancer mortality globally [1]. There are two main types of esophageal cancer: adenocarcinoma (EAC) and squamous cell carcinoma (ESCC). While EAC is the most common type in the United States and Western Europe, ESCC is predominant worldwide with higher incidence reported in Asia and developing countries [2; 3]. Epigenetic studies have revealed that EAC is strongly associated with gastroesophageal reflux disease and Barrett's esophagus whereas the risk factors for ESCC include alcohol consumption [4], smoking [5], dietary zinc deficiency [6], and mechanical insults [7]. Since there are no obvious symptoms during the early stages of EC, most patients especially ESCC patients are diagnosed late which leaves the individual with limited treatment options. Chemotherapy is the main treatment option for ESCC patients with cisplatin, 5-fluorouracil, paclitaxel, or the combination being routinely used [8]. Additionally, newer agents such as afatinib and bevacizumab, are under evaluation in clinical trials [9]. Despite the advances made in mechanistic understanding of the carcinogenesis and tumorigenesis of ESCC and new drug development, the 5-year survival rate of EC patients is still below 20% [10]. Design and development of novel chemotherapeutics to increase the overall and recurrence free survival rate continues to be an active area of research.

Store operated Ca^{2+} entry (SOCE) is an essential intracellular Ca^{2+} signaling pathway and plays an important role in tumor cell proliferation, migration, metastasis, invasion, and resistance to apoptosis [11]. There are two main family of proteins involved in SOCE in mammalian cells; stromal-interacting molecule family (STIM 1 and 2), and Orai (Orai1, Orai2 and Orai3). During activation of SOCE, depletion of ER Ca^{2+} stores serves as a signal to trigger translocation of STIM1 to ER-plasma membrane junctions where they conjugate with Orai and subsequently activated to allow extracellular Ca^{2+} influx into the cytoplasm [12]. Yang, *et al.* provided the first report on the role of STIM1 and Orai1 in breast cancer migration and metastasis [13]. Later, additional studies demonstrated that Orai1 and STIM1 have important functions in promoting cell proliferation, migration, invasion and apoptotic resistance in many types of cancers [14] such as ESCC [15], pancreatic adenocarcinoma [16], prostate cancer [17] and hepatocellular carcinoma [18]. Further, expression of Orai1 was much higher in tumor tissues than that in adjacent non-tumorous epithelial tissues in ESCC patients and associated with a poor survival rate. Elevated Orai1 is responsible for hyperactivity of intracellular Ca^{2+} oscillations and rampant cell proliferation in ESCC cells. Similarly, over-expression of STIM2 was observed in colorectal tumors and melanoma cells [19]. Up-regulation of Orai3 has been demonstrated in breast cancer tissues and cell lines such as MCF-7 and T47D [20].

Anti-tumor activity of skf-96765, a tool compound with non-specific activity against SOCE, in animal models of breast further established the role of SOCE in cancer [13]. Previous work from our lab demonstrated that skf-96765 inhibited Orai1-mediated intracellular Ca^{2+}

oscillations, proliferation of ESCC cells, and tumor growth *in vivo* [15]. RP4010 is a novel, oral inhibitor of Orai1 channel developed by Rhizen Pharmaceuticals and currently in Phase I/IB clinical development. Herein, we examined the anti-proliferative effects of RP4010 and the possible underlying mechanism in cultured human ESCC cells as well as an ESCC xenograft mouse model.

Materials and methods

Materials

RP4010 was supplied by Rhizen Pharmaceuticals, SA. Compound was dissolved in DMSO to make up a 10 mM stock solution. Human ESCC (KYSE-30, KYSE-150, KYSE-790 and KYSE-190), normal epithelial (HET-1A), lung cancer (A549) and ovarian cancer (A2780 and A2780-DX) cell lines were used in this study [15].

Cell culture

All cell lines were cultured in 37 °C, 5% CO_2 incubator. HET-1A cells were maintained in serum-free EpiCam medium (ATCC, US). ESCC cell lines (KYSE-30, KYSE-150, KYSE-790 and KYSE-190) were maintained in 1:1 mixture of RPMI-1640 medium and Ham's F12 Medium (Corning, US) supplemented with 5% fetal bovine serum (FBS, VWR, US) and 1% penicillin/streptomycin (Corning, US). During experiments, cells were cultured in experimental medium containing 1:1 RPMI-1640/Ham's F12, 5% FBS and antibiotics. A549, A2780 and A2780-DX cells were cultured in RPMI-1640 medium supplemented with 10% FBS.

Western blot

KYSE-150 cells were treated with different dose of RP4010 for the indicated times. Cells were lysed with RIPA buffer (150 mM NaCl, 50 mM Tris-Cl, 1 mM EGTA, 1% Triton X-100, 0.1% SDS and 1% sodium deoxycholate, pH 8.0) supplemented with proteinase inhibitor cocktail (Sigma-Aldrich, US). Protein concentration was quantified using a BCA kit (Thermo, US). Primary antibodies used in this study included anti-STIM1 (1:500, BD Transduction), anti-Orai1 (1:1000, Millipore), anti-Cyclin B1 (1:1000, Cell Signaling Technology, US), anti-Cyclin D1 (1:1000, Cell Signaling Technology, US), anti-P27 (1:1000, Cell Signaling Technology, US), anti-STIM1 (1:1000, BD Transduction Laboratories, Clone 44), anti-Orai1 (1:1500, Millipore, against residues 22–40 of human protein, US), and anti-GAPDH (1:1000, GeneTex, US). Secondary antibodies included HRP-labeled goat anti-rabbit IgG (1:5000, Cell Signaling Technology, US) and anti-mouse IgG (1:5000, Cell Signaling Technology, US). Signals were detected on SpectraMax® i3 (Molecular Devices, CA).

Cell Cycle Analysis

Cells were seeded at density of 2×10^5/well in 6-well plates and cultured for 24 h. Following seeding, cells were treated with RP4010 at the indicated concentration for 24 h, trypsinized, washed with PBS, and vortexed gently to obtain a mono-dispersed cell suspension. Suspension was transferred to ice cold 70% ethanol and maintained at 4°C for 4 h. After centrifugation of the ethanol-suspended cells for 5 min at 300 ×g, the cell pellets were

washed and resuspended in PBS. Cell cycle was determined according to the instructions provided by the kit manufacturer (Thermo Fisher, US). Briefly, cell suspension was incubated with 50 μg/mL DNase-free RNase for 30 min. After PBS wash, cells were stained with propidium iodide (PI) solution containing DNase-free RNase A and a permeabilization reagent. FACS AriaIIu flow cytometer (BD Sciences, US) and CellQuest software (BD Sciences) were employed to determine the cell percentage distribution.

MTT assay

KYSE-30 and KYSE-150 cells were seeded in a 96-well plate and incubated with RP4010 for 24 h, 48 h and 72 h, respectively. Cells were kept in the medium containing 10% of 3-(4, 5-dimethylthiazol-2-yl)-2, 5-diphenyl-tetrazolium bromide (MTT, 5 mg/ml) at 37 °C for 4 h. After removing the supernatant, formazan was dissolved in 150 μl DMSO. Absorbance was measured at 570 nm on SpectraMax® i3 (Molecular Devices, CA). IC_{50} of RP4010 were calculated using Graphpad Prism 5.

SOCE Measurement

KYSE-150 cells were seeded in glass-bottom dishes (Bioptechs, US) and cultured for 24 h, followed by 10 μM RP4010 treatment for 0.2 h, 2 h and 4 h. As described previously [21], the cells were loaded with 5 μM Fura-2 AM ester (Biotum, US) at 37°C for 45 min. Intracellular Ca^{2+} was measured by the fluorescence microscope with a SuperFluo 40× objective (Nikon, Japan) that was connected to a dual-wavelength spectrofluorometer (excitation λ = 350/385 nm and emission λ = 510 nm; Photon Technology International, NJ). Cellular ER Ca^{2+} stores were depleted by 10 μM thapsigargin (TG) prepared with BSS-0Ca^{2+} solution (in mM: 140 NaCl, 2.8 KCl, 2 MgCl2, 10 HEPES, pH 7.2, 0.5 mM EGTA). SOCE was observed upon the rapid exchange of extracellular solution to BSS-2Ca^{2+} (same as BSS-0Ca^{2+}, except 2 mM $CaCl_2$ to replace 0.5 mM EGTA). RP4010 treatment at the indicated concentration and time were applied to examine its effects on SOCE according to the experiments. SOCE activity is presented as the difference between basal and maximal values of F350/F385 (ΔF350/F385) after addition of 2 mM $CaCl_2$ in BSS solution.

Intracellular Ca^{2+} oscillations measurement

KYSE-150 cells were loaded with 3 μM Fluo-4 in 96-well imaging plates (BD Falcon, NJ) at 37 °C for 30 min. After washing, cells were kept in culture medium without phenol red. The intensity of fluorescent signals were recorded by Hamamatsu digital camera C11440 complemented with DMi8 inverted microscope (Leica, Germany) with 20× objective (dry lens, NA 0.75). Time lapse live cell images were recorded every 4 s for 3 min and analyzed using ImageJ.

Confocal imaging and NF-κB/p65 nuclei translocation assay

All cells were seeded on a cover slide coated with 0.01% Poly-L-Lysine (Trevigen, US). KYSE-150 cells were co-transfected with plasmids containing STIM1 fused with mOrange and Orai1 fused with GFP. After 36 h, the cells were treated with RP4010 or vehicle for 4 h followed by 10 μM TG to deplete ER Ca^{2+} stores and activate SOCE. Zeiss LSM 780 laser

scanning confocal microscope with 63× objective (NA 1.4, Zeiss, Germany) was used to visualize the co-localization of STIM1 and Orai1. For NF-κB/p65 imaging, all cells were starved in medium containing 0.1% FBS for 24-hours. Cells were stimulated by addition of 10% FBS for 60 min. Vehicle control, 20 μM BTP-2, or 10 μM RP4010 were added into both the starvation and stimulation medium. Cells were fixed using 4% paraformaldehyde in PBS and permeabilized by 0.1% Triton X-100. After incubation with 10% goat serum blocking solution for 30 min, cells were incubated with the primary antibody, i.e. rabbit anti-NF-κB/p65 (1:50, Santa Cruz, # sc-109) at 4 °C overnight. A goat anti-rabbit IgG-Alexa 488 (Abcam, # ab150077) was used as secondary antibody and incubated with cells for 1 h at room temperature. Hoechst 33342 (Enzo, # ENZ52401) was used to stain nuclei. For NF-κB/p65 translocation study, DMi8 inverted fluorescent microscope with 40× objective (NA1.3, Leica, Germany) was used.

Xenograft tumor growth assay

Animals care and experiments were approved by the Institutional Animal Care and Utilization Committee (IACUC). 100 μL PBS contained 1×10^6 KYSE-150 cells was mixed with an equal volume matrigel (Corning, US), followed by subcutaneously injected into the back of 6-week old male NCr nu/nu nude mouse (Taconic Farm, NY). One week later, tumors were visible, and mice were randomly assigned into different groups. Mice were treated with DMSO or RP4010 at indicated doses by intraperitoneal injection. Tumor volumes and body weights were collected every other day during the treatment period. Tumor volume (mm^3) was calculated using the following formula: Volume = $(\text{width})^2 \times \text{length} \times 3.14/6$. At the end of experiment, mice were euthanized and tumor and all the vital organs were collected.

H&E Staining

Post extraction, tissues were immediately fixed in 10% neutral buffered formalin for 48 h at 4°C and stained using a standard H&E protocol. After paraffin embedding, dewaxing and hydration, the tissue slides were processed as follows: hematoxylin solution staining for 3 min, DDW water wash for 1 min, incubated in 1% HCL-ethanol for 30 s, DDW water wash for 1 min, 1% ammonia solution for 10 s, DDW water wash for 1 min, eosin solution staining for 10 min, DDW water wash for 1 min, 70% ethanol for 30 s, 80% ethanol for 1 min, 95% ethanol I for 1 min, 95% ethanol II for 1 min, 100% ethanol I for 2 min, 100% ethanol II for 2 min, ethanol : dimethylbenzene (1:1) for 5 min, dimethylbenzene I for 5 min, dimethylbenzene II for 5 min, and finally sealed with neutral balsam and observed under microscope.

Immunofluorescence staining

After dissected, tumor tissues were mounted in OCT embedding compound and freeze at −80 °C. the cryostat sections were prepared by cutting the tissues at the thickness of 5 μ m using cryostat microtome (Leica, Germany). The slides were fixed in 4% formalin solution for 10 min and washed with PBS for 3 times. Then the slides were incubated with PBS containing 0.1 % Triton X-100 for 10 min and wash in PBS 3 times. Incubate the slides with 10% horse serum in PBST (0.1% Tween 20) for 30 min to block the unspecific binding of the antibodies. The primary antibodies which targeted NF-κB/p65 (1:50, Santa Cruz, #

sc-109) and cyclin D1 (1:100, abcam, ab134175, US) were employed at 4°C overnight. The slides were washed 3 times in PBS and incubated with secondary antibody which conjugated with Alexa 488 (1:1000, Abcam, # ab150077, US) for 1 h at room temperature in the dark. The slides were washed with PBS and stained with Hoechst 33342 (Enzo, # ENZ52401) to visualize the nuclei. After mounted with mounting medium, the slides were imaged using microscope with 20× and 40× objective (NA1.3, Leica, Germany).

Statistical Analysis

Statistical analyses were performed using Prism 5 (GraphPad, San Diego, CA). Data are presented as the mean ± standard deviation (SD). Significant differences were considered significant at a P value < 0.05 in all cases.

In animal experiment, there were 5 nude mice in each group of RP4010 and control. In tumor volume and body weight analysis, one-way analysis of variance (ANOVA) was applied to evaluate the significance among groups. Two tail t-test was employed to evaluate the significance of tumor weight in the RP4010 and control groups.

Two tail t-test was used in the analysis of significance between control and RP4010 groups on the cells in the phase of G0/G1 or G2/M (Fig. 2), cells with oscillations (Fig. 3), SOCE measurement (Fig. 2, Fig. 4, and Fig. S3), relative migration (Fig. S2) and protein expression level (Fig. S4). * $p<0.05$, ** $p<0.01$, *** $p<0.001$.

Results

RP4010 inhibited the proliferation of ESCC cells

MTT assays were performed to evaluate the anti-cancer efficacy of RP4010 in cultured human ESCC cell lines. As shown in Fig. 1A, treatment of RP4010 for 72 h reduced viability of all cell lines in a dose-dependent manner. The IC_{50} of RP4010 for KYSE-30, KYSE-70, KYSE-150, and KYSE-790 were 1.244, 1.412, 1.402, and 5.545 μM, respectively. Treatment with RP4010 reduced cell viability in a time-dependent manner (Fig. 1B and Fig. 1C). RP4010 achieved better inhibitory effect on KYSE-30 and KYSE-150 cell lines at 72 h than at 24 h or 48 h. The IC_{50} of 3,5-bis (trifluoromethyl) pyrazole (BTP-2) [22], a well-studied SOCE inhibitor were calculated as 17.78 and 17.71 μM for KYSE-30 and KYSE-150, respectively (Supplementary Materials, Fig. S1A and S1B). Data demonstrate the growth-inhibitory potential of RP4010 in ESCC cells.

Cell cycle arrested at G0/G1 phase in ESCC cells treated with RP4010

Next, we examined whether the anti-proliferative effect of RP4010 is through its effect on the cell cycle. Live cell imaging of KYSE-150 cells treated with 10 μM RP4010 for 48 h was performed. PI, a cell membrane non-permeable DNA dye was used to stain nuclei of cells undergoing necrosis or late apoptosis; Hoechst 33342, a cell membrane-permeable dye was used to reveal all nuclei. As shown in Fig. 2A, the RP4010 treated cells displayed almost no positive PI signal while MK2206, a known AKT inhibitor with highly cytotoxic manifested by increased PI stained (red) nuclei in majority of the cells. Hoechst 33342 images failed to reveal any apoptotic hallmarks, such as nuclear condensation or

fragmentation in KYSE-150 cells treated with RP4010. Data suggest that RP4010 did not induce cell death in ESCC cells. We then performed cell cycle analysis in KYSE-150 cells treated with or without RP4010 using flow cytometry. As shown in Fig. 2B & C, approximately 80% of KYSE-150 cells were at G0/G1 phase in RP4010 (10μM) treatment group whereas this number for control non-treatment group was only 56%. Additionally, treatment with both 2 and 10 μM RP4010 significantly reduced cell numbers in G2/M phase. Western blot analysis further indicated that the protein level of $P27^{Kip1}$, an inhibitor for cyclin-Cdk [23], was increased in cells treated with RP4010 especially at higher concentrations (Fig. 2D). Two other important cell cycle regulatory proteins, cyclin B1 and cyclin D1, were dramatically decreased in KYSE-150 cells treated with RP4010 at 2 and 10 μM (Fig. 2D). Data suggest that treatment with RP4010 induces cell cycle arrest at G0/G1 phase but does not result in death of ESCC cells.

SOCE and Ca^{2+} oscillations were blocked by RP4010 in ESCC cells

We previously demonstrated that SOCE-mediated intracellular Ca^{2+} oscillations were essential for cell proliferation in ESCC cells [15]. Therefore, we tested whether the anti-proliferation function of RP4010 could be *via* blockade of SOCE and SOCE-mediated intracellular Ca^{2+} oscillations. KYSE-150 cells were treated with or without 10 μM RP4010 for 0.2, 2, and 4 h, respectively. ER Ca^{2+} store was depleted by thapsigargin (TG) in BSS-0Ca^{2+}solution, which was displayed as the first peak of ratio of fura-2 fluorescence with excitation wavelength at 350/385 nm and emission wavelength at 510nm (Fig. 3A). Once extracellular solution was changed to BSS-2Ca^{2+}, SOCE was induced (second peak of F350/F385). Relative SOCE in each group was calculated as the difference in F350/F385 before addition of BSS-2Ca^{2+} and the peak value (Fig. 3B). While BSS-2Ca^{2+} solution containing RP4010 (10 μM) failed to inhibit SOCE, pre-incubation of RP4010 for 2 h and 4 h significantly inhibited SOCE in KYSE-150 cells compared to the control (Fig. 3A and B). Similarly, pre-incubation of RP4010 for 4 h significantly inhibited SOCE in other cancer cell lines, such as KYSE-150, KYSE-720, A549, A2780 as well as the doxorubicin resistant A2780-DX cells (Supplementary Materials, Fig. S3). Intracellular Ca^{2+} oscillations experiments were performed in KYSE-150 cells pre-incubated with RP4010 (10 μM) for 4 h. Cells were loaded with Fluo-4 AM and fluorescent live cell imaging was performed in these cells in culture medium without phenol red at 37°C supplemented with 5% CO_2. KYSE-150 cells presented spontaneous intracellular Ca^{2+} oscillations in control group (upper panels, Fig. 3C) but absent in RP4010 treated cells (lower panels, Fig. 3C). A representative sinusoidal curve of Ca^{2+} oscillations was observed in the control group of KYSE-150 cells (Fig. 3D). While 80% of cells demonstrated intracellular Ca^{2+} oscillations in control group, only 15% of cells did so in RP4010 treatment group (Fig. 3E). Similar results were observed in other ESCC cell lines (not shown). Clearly, these data demonstrated that RP4010 significantly blocked SOCE and SOCE-mediated intracellular Ca^{2+} oscillations in ESCC cells.

RP4010 had no impact on the expression or translocation of Orai1 but inhibited translocation of NF-κB/p65 to nuclei

We examined the mechanism underlying inhibitory function of RP4010 on SOCE and the proliferation of ESCC cells. Since the “kick-in” time for RP4010 was more than 2 hours, we

first studied whether the expression of STIM1 or Orai1 proteins was down-regulated. Western blot images failed to show any reduction of protein expression of these proteins (Fig. 4A). Next, we investigated whether RP4010 could interrupt the translocation of Orai1. KYSE-150 cells were co-transfected with plasmids containing STIM1 fused with mOrange and Orai1 fused with GFP. After ER Ca^{2+} stores were depleted by 10 μM TG, colocalized "puncta" of both STIM1 and Orai1 were observed in both untreated and RP4010 treated cells (Fig. 4B). Subsequently, a KYSE-150 cell line stably expressing shRNA to knockdown Orai1 was transfected with plasmid containing $Orai1^{V102C}$, a constitutive activated mutant of Orai1 channel. As shown in Fig. 4C and 4D, treatment of RP4010 (10 μM) was still able to inhibit SOCE. Data suggest that the mechanism underlying the inhibitory function of RP4010 may not through interrupting STIM1-Orai1 interaction or translocation of Orai1.

Several transcription factors have been demonstrated to be involved in intracellular Ca^{2+} oscillations mediated proliferation signaling pathways. Since RP4010 inhibited SOCE and intracellular Ca^{2+} oscillations, we investigated whether RP4010 could block nuclear factor kappa B (NF-κB/p65) nuclear translocation upon serum stimulation in ESCC cells. KYSE-150 cells were starved in medium supplemented with 0.1% FBS for 24 h. Under starvation, the fluorescent signal of NF-κB/p65 (green) displayed almost exclusively in cytosol without co-localization with Hoechst 33342-stained nuclei (pseudo color of red) (Fig. 5A). Upon 10% FBS stimulation for 1 h, NF-κB/p65 appeared to translocate to nuclei evidenced by co-localization of nuclei in about 84% of KYSE-150 cells (Fig. 5B, left panels). Treatment with either 20 μM BTP-2 or 10 μM RP4010 reduced the number of cells with NF-κB/p65 nuclear localization to 8.53% and 10.52%, respectively. Besides NF-κB pathway, we also examined Akt and ERK pathways and found that RP4010 did not alter these pathways in KYSE-150 cells (Supplementary Materials, Fig. S4A and S4B). In consistent with *in vitro* studies, immunofluorescence staining of tumor tissues also demonstrated that nuclear NF-κB/p65 positive cells number was only 9% in RP4010 group compared with 41% in control animals (Fig. 5C); the expression of cyclin D1 which was a target of NF-κB/p65 was also dramatically reduced in tumors removed from RP4010 treated animals compared with that removed from control group (Fig. 5D). Data therefore indicate a role for RP4010 in the NF-κB/p65 signaling pathway both *in vivo* and *in vitro*.

RP4010 inhibits tumor growth in xenografted mice

Lastly, we evaluated the anti-cancer effect of RP4010 in ESCC xenograft nude mice. One week after inoculation of 1×10^6 KYSE-150 cells and development of visible tumors, mice were randomly assigned into vehicle control and RP4010 treatment (20 mg/kg, i.p. injection every 2 days for 2 weeks) groups. There were no differences in terms of body weight between the two groups (Fig. 6B). Compared with control group, RP4010 treatment group demonstrated significantly slower tumor growth (Fig. 6A). At the end of the study, tumors were dissected from mice followed by imaging and measurement of the tumor size. Results showed that the volume and weights of tumors from RP4010 treated animals were significantly less than those of the control group (Fig. 6C and D). H&E staining of the heart, spleen, liver and kidney collected from the RP4010 treatment group showed no obvious toxicity, with similar histology features as control group (Fig. 6E). Pathology images from tumors revealed that a significant portion of tumors in both group were undergoing necrosis.

While typical squamous cells carcinoma feature was clearly presented in tumors removed from control group, interestingly, the feature was missing in tumors harvested from RP4010 treated mice (Fig. 6E, right panels). Collectively, the *in vivo* data suggest that RP4010 could inhibit the tumor growth in xenograft ESCC nude mice without any obvious toxicity to vital organs.

Discussion

SOCE-mediated intracellular Ca^{2+} signaling regulates many cellular events in various cells such as proliferation, migration, and invasion. In this study, we demonstrated that RP4010, a new oral SOCE channel inhibitor currently in Phase I/IB clinical development, could effectively block SOCE and cell proliferation in ESCC cells. Treatment of RP4010 (10 μM) inhibited intracellular Ca^{2+} oscillations, halted Ca^{2+}-dependent nuclear translocation of NF-κB, and resulted in cell cycles arrested at G0/G1 phase. Interestingly, RP4010 did not induce significant cell death even at rather high concentrations. *In vivo* study revealed that the mice tolerated I.P. injection of 20 mg/kg RP4010 every two days without body weight loss or noticeable adverse effects up to 4 weeks. At this dose, RP4010 significantly reduced ESCC tumor growth compared to vehicle treated control group.

For several years, investigators have devoted their efforts to the discovery and development of potent, specific and safe SOCE inhibitors for clinical applications. For example, AnCoA4 was identified as a new SOCE inhibitor by using minimal functional domains of STIM1 and Orai1 in microarrays for small-molecule compounds binding screening [24]. To overcome the non-selective and multi-target nature of a well-studied SOCE inhibitor 2-APB, the dimer forms of 2-APB, e.g. DPB-162AE and DPB-163AE were constructed with 100-fold potency compared to 2-APB without affecting IP3R function [11]. Targeting the pore geometry, especially the Ca^{2+} selectivity filter of Orai1 channel, another class of inhibitors of Orai1 were synthesized including SB01990, SPB06836, KM06293 and RH01882. Pyrazole compounds such as Pyr2 (also known as BTP-2), 3, 6 and 10, demonstrated differential selectivity on TRPC3 and Orai1/STIM1-mediated SOCE. Inhibitory effects of RP4010 on SOCE were evident only after pre-incubation with ESCC cells for more than 2 hours. Many of SOCE inhibitors require pre-incubation time ranging from a few minutes to hours [25]. Being a slow process, RP4010 could act against STIM1 oligomerisation, and/or STIM1-Orai1 coupling, and/or Orai1 activation. Although RP4010 has no effect on the expression of STIM1 or Orai1 nor on the STIM1-Orai1 translocation and interaction, the possibility that the SOCE inhibition is due to secondary effects of RP4010 cannot be ruled out. The exact mechanism underlying the inhibitory function of RP4010 on Orai1 require further investigation.

Compared to the commonly used BTP-2, RP4010 was more potent with respect to inhibition of ESCC cell proliferation. IC_{50} of RP4010 in cell viability assays were 1.2–5 μM while the IC_{50} of BTP-2 was one order higher (Supplementary Materials, Fig. S1). Interestingly, RP4010 inhibited cell proliferation not only in ESCC cell lines, but also in other cancer cell lines, including lung cancer (A549), ovarian cancer (A2780) and even the doxorubicin resistant A2780-DX cells (Supplementary Materials, Fig. S3). Data suggest that RP4010 could inhibit a common SOCE pathway in various cancers and may have useful application

in cancer cells that have developed drug-resistance. It is noteworthy that RP4010 treatment results in cell cycle arrest but does not cause cell death even at concentrations as high as 30 μM, which is unlike other SOCE inhibitors (skf-96765, 2-APB, BTP-2, our unpublished observations) [26]. Since ESCC cells require higher Orai1-mediated SOCE to support their fast proliferation compared to normal epithelial cells, inhibiting to data suggest that RP4010 may be tumor specific while sparing healthy cells.

We previously demonstrated that Orai1-mediated intracellular Ca^{2+} oscillations are essential for cell proliferation in ESCC [15]. The frequency, amplitude, and duration of the intracellular Ca^{2+} oscillations compose the specific Ca^{2+} codes for selective activation of transcription factors for gene transcription, cell proliferation and migration [27; 28; 29]. The decoding of the oscillatory form is achieved by intracellular downstream effectors, such as calmodulin (CaM), nuclear factor of activated T-cells (NFAT), NF-κB, CaM-dependent protein kinase II (CaMKII), that differ in their on- and off-rates for Ca^{2+} and subsequently activate different cellular processes [14]. Intracellular Ca^{2+} oscillations can reduce the effective Ca^{2+} threshold for signaling transduction, thereby increasing signal detection at low levels of stimulation. The intracellular Ca^{2+} oscillations-regulated transcription factor has been studied very well in lymphocytes, which is through the NFAT pathway. However, the Ca^{2+} oscillations-regulated transcription factor in cancer cells remains largely unknown. The NF-κB is a family of transcription factors (p50, p52, p65/RelA, c-Rel, and RelB) important for cell proliferation, transformation, and tumor development [30]. Once it is activated, NF-κB/p65 is released from cytoplasmic IκB and translocates to the nucleus [31]. As shown Fig. 5, RP4010 blocked the translocation of NF-κB from cytosol to nuclei in ESCC cells. It has been reported that serum-induced intracellular Ca^{2+} oscillations are critical for NF-κB activation in 3T3 cells [32]. Consistent with that report, RP4010 likely blocked nuclear translocation of NF-κB by inhibiting SOCE-mediated intracellular Ca^{2+} oscillations. Cyclins, including cyclin B1 and cyclin D1, are two among many of NF-κB targeted genes [33; 34]. Both i*n vitro* and *in vivo* evidence showed that the expression levels of cyclin B1 and cyclin D1 were dramatically reduced in ESCC cells (Fig. 2D) or tumors (Fig. 5D) treated with RP4010. Taking together, our data suggest that RP4010 can inhibit SOCE-mediated intracellular Ca^{2+} oscillations, which in turn resulted in cycle arrest and cell proliferation inhibition in ESCC cells.

In addition to uncontrolled proliferation, another hallmark of cancer cells is the ability to metastasize. In a wound healing assay, we found that RP4010 could significantly reduce the migration of ESCC (Supplementary Materials, Fig. S2 A and B). At a concentration of 25 μM, RP4010 completely inhibited the migration in all ESCC cells. E-cadherin, an important protein for formation of cell adherents junction, has been suggested as a tumor suppressor, loss of activity or expression of which is related to cancer progression and metastasis [35]. Vimentin, a type III intermediate filament protein, promotes cell mobility and is related with incidence of lymph node metastasis in esophagus cancer [36]. Treatment with RP4010 significantly reduced the expression of Vimentin besides increase E-cadherin level, consistent with the data from cell migration assay (Supplementary Materials, Fig. S2C). Data therefore indicate that RP4010 may inhibit the metastasis of ESCC cells.

In conclusion, this study demonstrated the SOCE-blocking ability of a novel compound, RP4010. Inhibition of intracellular Ca^{2+} oscillations and NF-μB nuclear translocation resulted in a subsequent attenuation of ESCC cell proliferation, migration, as well as tumor growth *in vivo*. While the current study suggests RP4010 may be a potential chemotherapy or adjuvant drug for chemotherapy for ESCC, further investigation is needed to understand the exact nature of binding with the individual SOCE channel proteins.

Supplementary Material

Refer to Web version on PubMed Central for supplementary material.

Acknowledgments

This work was supported by U.S. National Institutes of Health (NIH) National Cancer Institute Grant R01-CA185055 and University of Texas System STARs award (to ZP).

Nonstandard abbreviations

EC	esophageal cancer
SOCE	store-operated Ca^{2+} entry
EAC	esophageal adenocarcinoma
ESCC	esophageal squamous cell carcinoma
STIM	stromal-interacting molecule
TG	thapsigargin
NF-κB	nuclear factor kappa B
BTP-2	3,5-bis (trifluoromethyl) pyrazole
2-APB	2-aminoethyl diphenylborinate
FBS	fetal bovine serum
MTT	3-(4, 5-dimethylthiazol-2-yl)-2, 5-diphenyl-tetrazolium bromide

References

1. Pennathur A, Gibson MK, Jobe BA, Luketich JD. Oesophageal carcinoma. Lancet. 2013; 381:400–412. [PubMed: 23374478]
2. Wheeler JB, Reed CE. Epidemiology of Esophageal Cancer. Surgical Clinics of North America. 2012; 92:1077–1087. [PubMed: 23026270]
3. di Pietro M, Canto MI, Fitzgerald RC. Endoscopic Management of Early Adenocarcinoma and Squamous Cell Carcinoma of the Esophagus: Screening, Diagnosis, and Therapy. Gastroenterology. 2017
4. Brooks PJ, Enoch MA, Goldman D, Li TK, Yokoyama A. The alcohol flushing response: an unrecognized risk factor for esophageal cancer from alcohol consumption. PLoS medicine. 2009; 6:e50. [PubMed: 19320537]

5. Morita M, Kuwano H, Ohno S, Sugimachi K, Seo Y, Tomoda H, Furusawa M, Nakashima T. Multiple occurrence of carcinoma in the upper aerodigestive tract associated with esophageal cancer: reference to smoking, drinking and family history. International journal of cancer. 1994; 58:207–210. [PubMed: 8026883]

6. Choi S, Cui C, Luo Y, Kim SH, Ko JK, Huo X, Ma J, Fu LW, Souza RF, Korichneva I, Pan Z. Selective inhibitory effects of zinc on cell proliferation in esophageal squamous cell carcinoma through Orai1. FASEB journal : official publication of the Federation of American Societies for Experimental Biology. 2018; 32:404–416. [PubMed: 28928244]

7. Lambert R, Hainaut P. Esophageal cancer: cases and causes (part I). Endoscopy. 2007; 39:550–555. [PubMed: 17554654]

8. Jin J, Liao Z, Zhang Z, Ajani J, Swisher S, Chang JY, Jeter M, Guerrero T, Stevens CW, Vaporciyan A, Putnam J Jr, Walsh G, Smythe R, Roth J, Yao J, Allen P, Cox JD, Komaki R. Induction chemotherapy improved outcomes of patients with resectable esophageal cancer who received chemoradiotherapy followed by surgery. International journal of radiation oncology, biology, physics. 2004; 60:427–436.

9. Spicer J, Irshad S, Ang JE, Enting D, Kristeleit R, Uttenreuther-Fischer M, Pemberton K, Pelling K, Schnell D, de Bono J. A phase I study of afatinib combined with paclitaxel and bevacizumab in patients with advanced solid tumors. Cancer chemotherapy and pharmacology. 2017; 79:17–27. [PubMed: 27872953]

10. Siegel RL, Miller KD, Jemal A. Cancer Statistics, 2017. CA: a cancer journal for clinicians. 2017; 67:7–30. [PubMed: 28055103]

11. Cui C, Merritt R, Fu L, Pan Z. Targeting calcium signaling in cancer therapy. Acta pharmaceutica Sinica. B. 2017; 7:3–17. [PubMed: 28119804]

12. Bergmeier W, Weidinger C, Zee I, Feske S. Emerging roles of store-operated Ca(2)(+) entry through STIM and ORAI proteins in immunity, hemostasis and cancer. Channels. 2013; 7:379–391. [PubMed: 23511024]

13. Yang S, Zhang JJ, Huang XY. Orai1 and STIM1 are critical for breast tumor cell migration and metastasis. Cancer Cell. 2009; 15:124–134. [PubMed: 19185847]

14. Pan Z, Ma J. Open Sesame: treasure in store-operated calcium entry pathway for cancer therapy. Science China. Life sciences. 2015; 58:48–53. [PubMed: 25481035]

15. Zhu H, Zhang H, Jin F, Fang M, Huang M, Yang CS, Chen T, Fu L, Pan Z. Elevated Orai1 expression mediates tumor-promoting intracellular Ca2+ oscillations in human esophageal squamous cell carcinoma. Oncotarget. 2014; 5:3455–3471. [PubMed: 24797725]

16. Kondratska K, Kondratskyi A, Yassine M, Lemonnier L, Lepage G, Morabito A, Skryma R, Prevarskaya N. Orai1 and STIM1 mediate SOCE and contribute to apoptotic resistance of pancreatic adenocarcinoma. Biochimica et biophysica acta. 2014; 1843:2263–2269. [PubMed: 24583265]

17. Flourakis M, Lehen'kyi V, Beck B, Raphael M, Vandenberghe M, Abeele FV, Roudbaraki M, Lepage G, Mauroy B, Romanin C, Shuba Y, Skryma R, Prevarskaya N. Orai1 contributes to the establishment of an apoptosis-resistant phenotype in prostate cancer cells. Cell death & disease. 2010; 1:e75. [PubMed: 21364678]

18. Yang N, Tang Y, Wang F, Zhang H, Xu D, Shen Y, Sun S, Yang G. Blockade of store-operated Ca(2+) entry inhibits hepatocarcinoma cell migration and invasion by regulating focal adhesion turnover. Cancer Lett. 2013; 330:163–169. [PubMed: 23211538]

19. Aytes A, Mollevi DG, Martinez-Iniesta M, Nadal M, Vidal A, Morales A, Salazar R, Capella G, Villanueva A. Stromal interaction molecule 2 (STIM2) is frequently overexpressed in colorectal tumors and confers a tumor cell growth suppressor phenotype. Molecular carcinogenesis. 2012; 51:746–753. [PubMed: 22125164]

20. Motiani RK, Zhang X, Harmon KE, Keller RS, Matrougui K, Bennett JA, Trebak M. Orai3 is an estrogen receptor alpha-regulated Ca(2)(+) channel that promotes tumorigenesis. FASEB journal : official publication of the Federation of American Societies for Experimental Biology. 2013; 27:63–75. [PubMed: 22993197]

21. Pan Z, Zhao X, Brotto M. Fluorescence-based measurement of store-operated calcium entry in live cells: from cultured cancer cell to skeletal muscle fiber. Journal of visualized experiments : JoVE. 2012
22. Demczuk M, Huang H, White C, Kipp JL. Retinoic Acid Regulates Calcium Signaling to Promote Mouse Ovarian Granulosa Cell Proliferation. Biology of reproduction. 2016; 95:70. [PubMed: 27488031]
23. Polyak K, Kato JY, Solomon MJ, Sherr CJ, Massague J, Roberts JM, Koff A. p27Kip1, a cyclin-Cdk inhibitor, links transforming growth factor-beta and contact inhibition to cell cycle arrest. Genes & development. 1994; 8:9–22. [PubMed: 8288131]
24. Sadaghiani AM, Lee SM, Odegaard JI, Leveson-Gower DB, McPherson OM, Novick P, Kim MR, Koehler AN, Negrin R, Dolmetsch RE, Park CY. Identification of Orai1 channel inhibitors by using minimal functional domains to screen small molecule microarrays. Chemistry & biology. 2014; 21:1278–1292. [PubMed: 25308275]
25. Rahman S, Rahman T. Unveiling some FDA-approved drugs as inhibitors of the store-operated Ca(2+) entry pathway. Scientific reports. 2017; 7:12881. [PubMed: 29038464]
26. Liu H, Hughes JD, Rollins S, Chen B, Perkins E. Calcium entry via ORAI1 regulates glioblastoma cell proliferation and apoptosis. Exp Mol Pathol. 2011; 91:753–760. [PubMed: 21945734]
27. Parekh AB. Decoding cytosolic Ca2+ oscillations. Trends Biochem. Sci. 2011; 36:78–87. [PubMed: 20810284]
28. Berridge MJ. The AM and FM of calcium signalling. Nature. 1997; 386:759–760. [PubMed: 9126727]
29. Dolmetsch RE, Xu K, Lewis RS. Calcium oscillations increase the efficiency and specificity of gene expression. Nature. 1998; 392:933–936. [PubMed: 9582075]
30. Chapman NR, Webster GA, Gillespie PJ, Wilson BJ, Crouch DH, Perkins ND. A novel form of the RelA nuclear factor kappaB subunit is induced by and forms a complex with the proto-oncogene c-Myc. The Biochemical journal. 2002; 366:459–469. [PubMed: 12027803]
31. Baeuerle PA, Baltimore D. NF-kappa B: ten years after. Cell. 1996; 87:13–20. [PubMed: 8858144]
32. See V, Rajala NK, Spiller DG, White MR. Calcium-dependent regulation of the cell cycle via a novel MAPK--NF-kappaB pathway in Swiss 3T3 cells. The Journal of cell biology. 2004; 166:661–672. [PubMed: 15326199]
33. Hinz M, Krappmann D, Eichten A, Heder A, Scheidereit C, Strauss M. NF-kappaB function in growth control: regulation of cyclin D1 expression and G0/G1-to-S-phase transition. Molecular and cellular biology. 1999; 19:2690–2698. [PubMed: 10082535]
34. Chen X, Shen B, Xia L, Khaletzkiy A, Chu D, Wong JY, Li JJ. Activation of nuclear factor kappaB in radioresistance of TP53-inactive human keratinocytes. Cancer Res. 2002; 62:1213–1221. [PubMed: 11861406]
35. Semb H, Christofori G. The Tumor-Suppressor Function of E-Cadherin. The American Journal of Human Genetics. 1998; 63:1588–1593. [PubMed: 9837810]
36. Mendez MG, Kojima S-I, Goldman RD. Vimentin induces changes in cell shape, motility, and adhesion during the epithelial to mesenchymal transition. The FASEB Journal. 2010; 24:1838–1851. [PubMed: 20097873]

Highlights

- RP4010 is a novel and potent store-operated Ca^{2+} entry blocker.
- Reduction of intracellular Ca^{2+} oscillations by RP4010 can inhibit cell proliferation and arrest cell cycle at G0/G1 phase in human esophageal squamous cancer cells.
- Blocking nuclear translocation of NF-κB is involved in this pathway.
- RP4010 inhibits tumor growth in esophageal cancer xenograft mice with no obvious adverse effect.

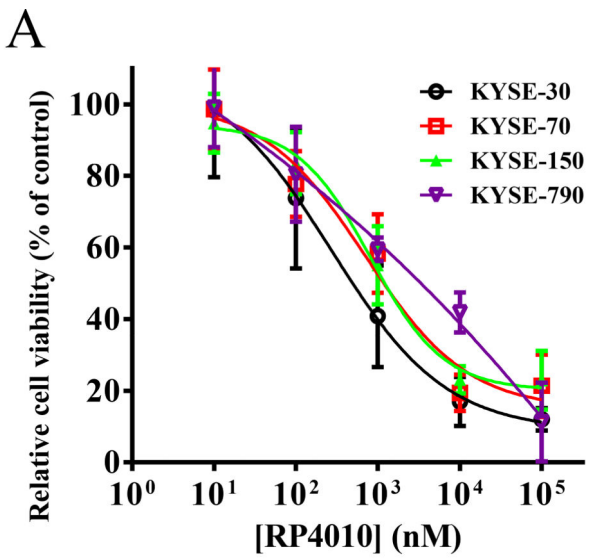

Cell line	KYSE-30	KYSE-70	KYSE-150	KYSE-790
IC_{50} (μM)	1.244	1.412	1.402	5.545

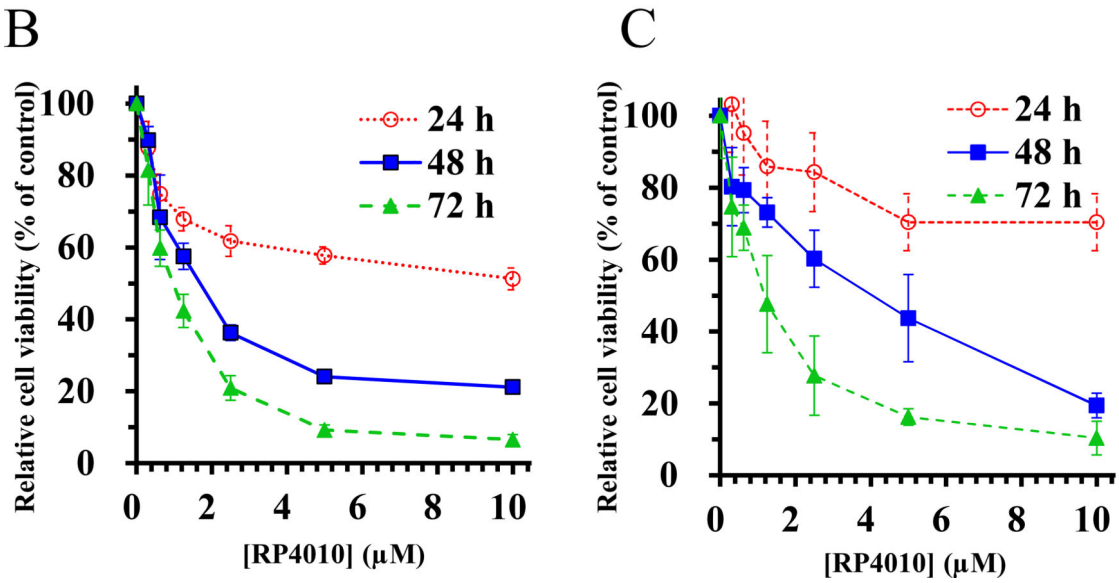

Figure 1.

RP4010 inhibited cell proliferation in cultured human ESCC cell lines. (A) Cell viability with or without RP4010 treatment after 72 h were calculated by MTT assay in ESCC cells, i.e. KYSE-30, KYSE-70, KYSE-150 and KYSE-790. The relative cell numbers were normalized with samples with vehicle control. Cell viability after 24 h, 48 h and 72 h in KYSE-30 (B) and KYSE-150 (C) are examined. Data were collected from two independent experiments and triplicates each time, Mean ± SD.

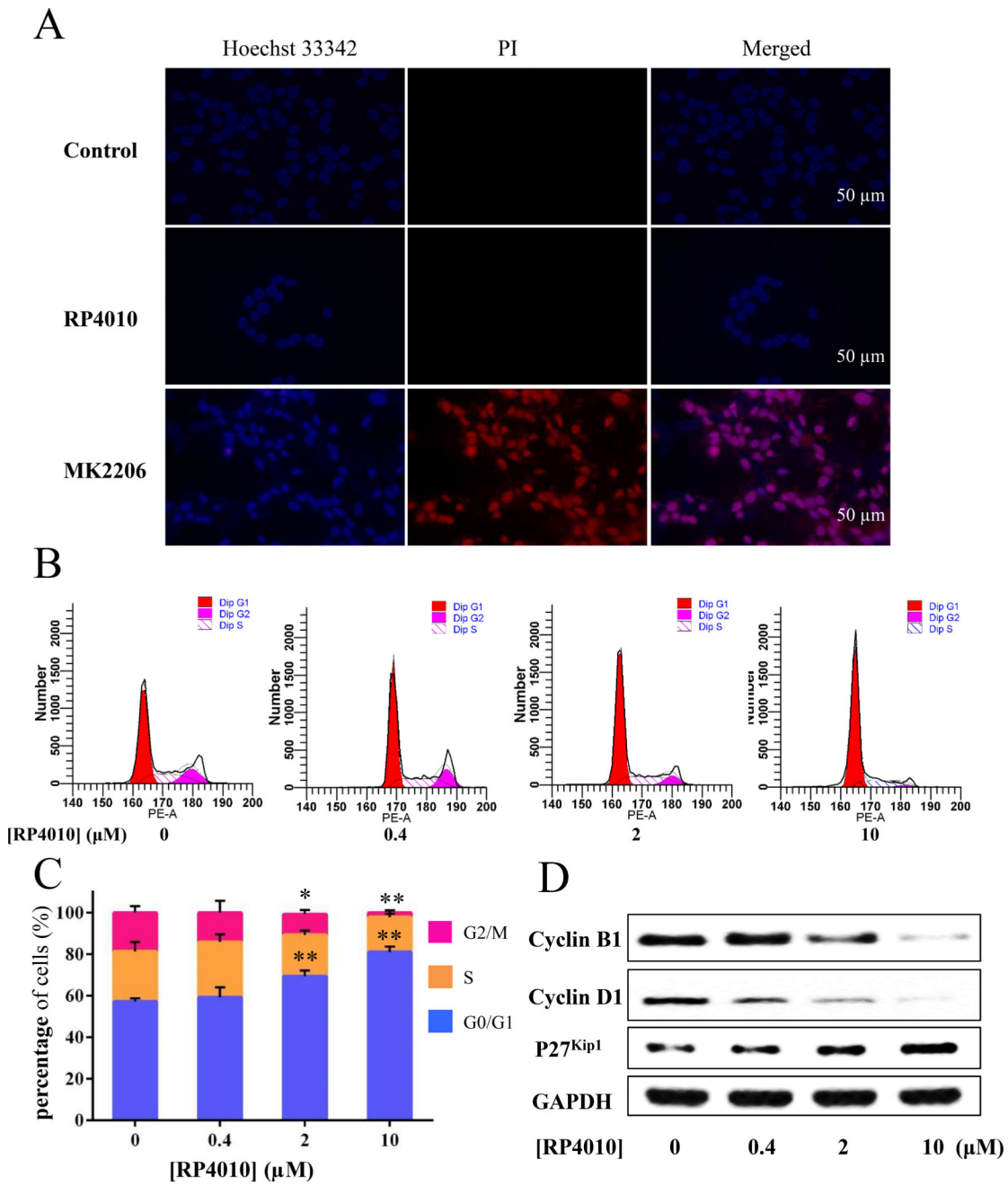

Figure 2.

Cell cycle was arrested at G0/G1 phase in KYSE-150 cells treated with RP4010. (A) Hoechst 33342 (blue) and PI (red) staining of KYSE-150 cells treated with vehicle (control), RP4010 (10 μM), or MK2206 for 48 hours. MK2206, an Akt inhibitor was used as positive control for cell death. (B) The populations of RP4010 treated KYSE-150 cells in G0, G1 and S phase were calculated by flow cytometry.(C) Statistical data of the percentage of G0/G1, S and G2/M phase in the KYSE-150 cells with RP4010 treatment at the concentration of 0, 0.4, 2 and 10 μM. (D) Western Blot of cell cycle related proteins, i.e. Cyclin B1, Cyclin D1 and P27 were performed in KYSE-150 cells treated with RP4010 at concentrations of 0, 0.4,

2 and 10 μM, respectively. GAPDH was used as a loading control. Data is showed as mean ± SD. **$p \leq 0.01$ and *$p \leq 0.05$.

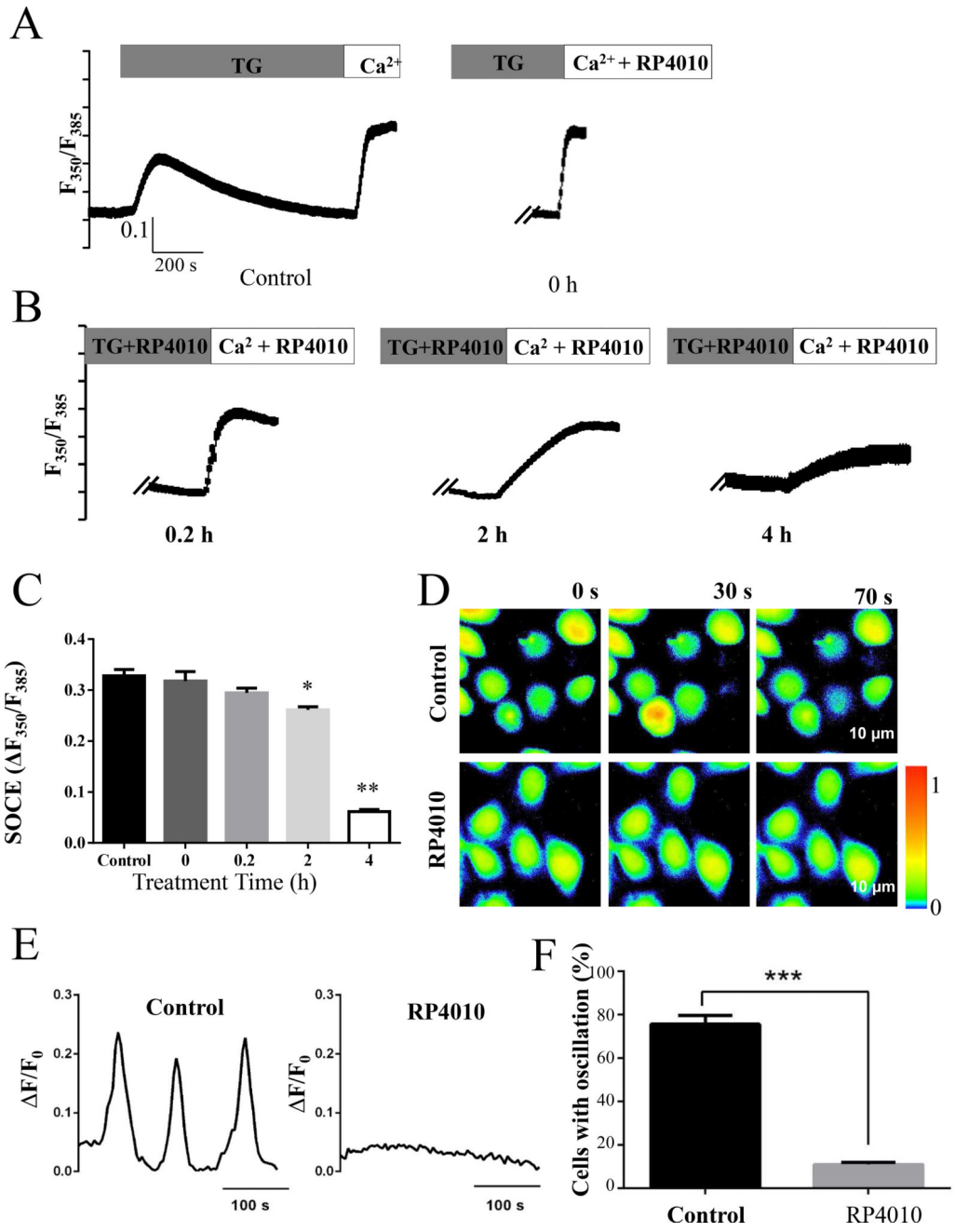

Figure 3.

SOCE and intracellular Ca^{2+} oscillations were blocked by RP4010. (A) SOCE was measured in KYSE-150 cells with vehicle (control) or with the treatment of 10 μM RP4010 for 0, 0.2, 2 and 4 hours. Intracellular Ca2+ concentration was represented by the fluorescent ratio of 350nm/385nm of Fura-2. (B) Summary of changes in SOCE in control or RP4010 treated for 0, 0.2. 2 and 4 h. (C) Representative Ca^{2+} probe Fluo-4 fluorescent live cell images in KYSE-150 cells treated with or without 10 μM RP4010. Scale bar, 75 μm. (D) Intracellular Ca^{2+} oscillations in control but not in RP4010 treated cells (plotted from C). (E) Statistics of cells with Ca^{2+} oscillations. Data are presented as mean ± SD. *** $p \leq 0.001$.

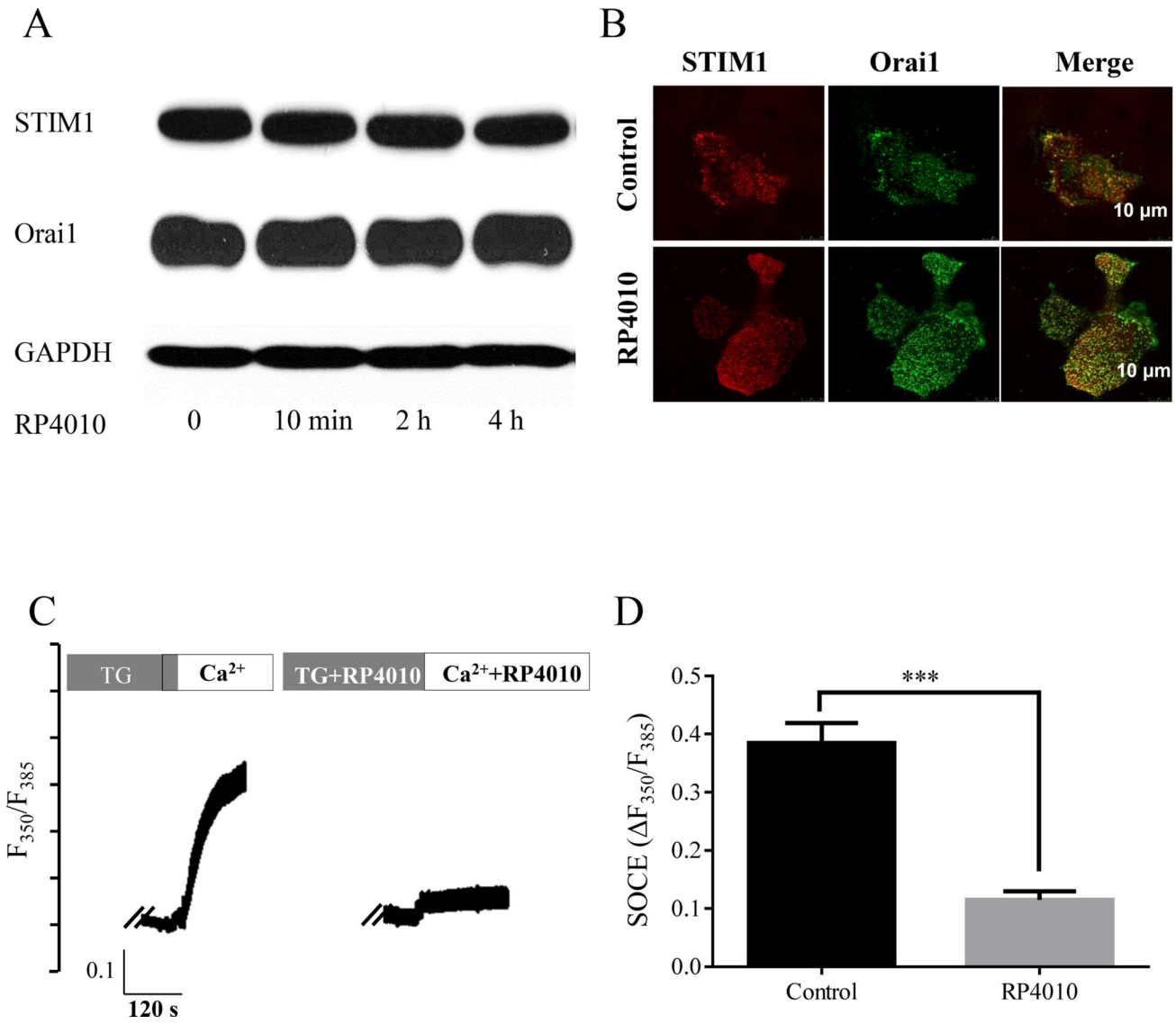

Figure 4.

Orai1 expression and translocation were not affected by RP4010. (A) Western blot of STIM1 and Orai1 was conducted in KYSE-150 cells with 10 μM RP4010 treatment for 10 min, 2 hours and 4 hours. (B) Confocal images of STIM1-mOrange and Orai1-GFP. KYSE-150 cells were treated with TG (10 μM) first to deplete ER Ca^{2+} stores and to activate SOCE. STIM1 and Orai1 could co-localize in control or RP4010 (10 μM) treated cells, but not cells treated with ML-9 (100 μM), a known SOCE inhibitor disrupting translocation of Orai1. Scale bar 10 μm. (C) SOCE in control and RP4010 (10 μM) treated KYSE-150 cells expressing Orai1 V102C, a constitutively active mutant. (D) Statistic of SOCE in cells expressing $Orai1^{V102C}$. Mean ± SD. ***$p \leq 0.001$.

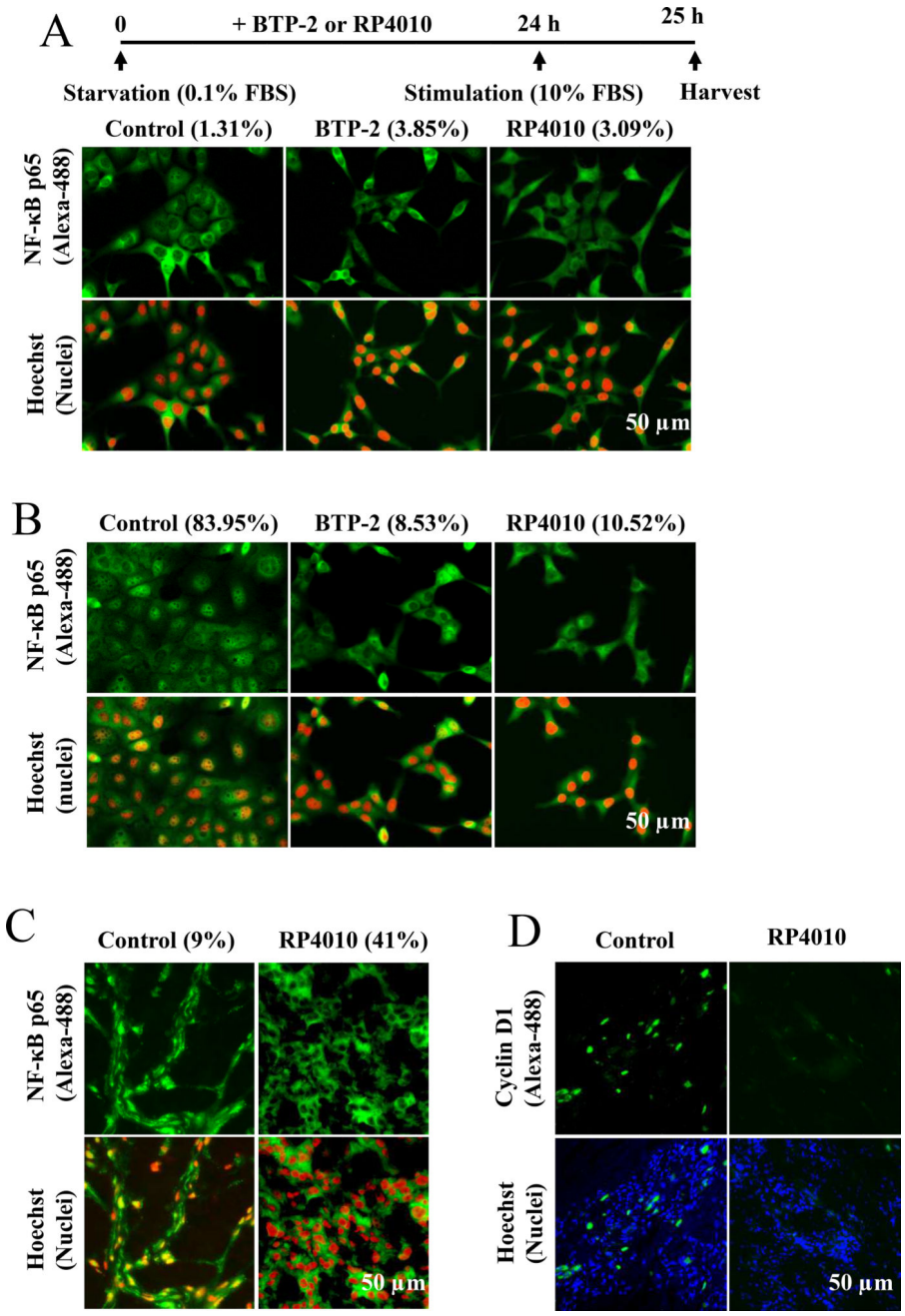

Figure 5.

RP4010 inhibited translocation of NF-κB/p65 to nuclei in *vitro* and in *vivo*. Immunostaining of NF-κB subunit p65 (green) and nuclei (red) in KYSE-150 cells undergoing starvation (A, culture medium containing 0.1 % FBS) or in proliferation (B, culture medium containing 10 % FBS induction). The percentage of cells with p65 nuclear translocation in each group is indicated in bracket. Scale bar, 50 μm. (C) Immunofluorescence staining of cryostat section of xenograft nude mice treated with and without RP4010 (control) were stained with NF-κB/ p65 antibody and nuclei dye (Hoechst). NF-κB/p65 signal was presented as green and nuclei as red. Scale bar, 50 μm. (D) Immunofluorescence staining of cryostat section of

xenograft nude mice treated with and without RP4010 (control) were stained with cyclin D1 antibody and nuclei dye (Hoechst). Cyclin D1 signal was presented as green and nuclei as blue. Scale bar, 50 μm.

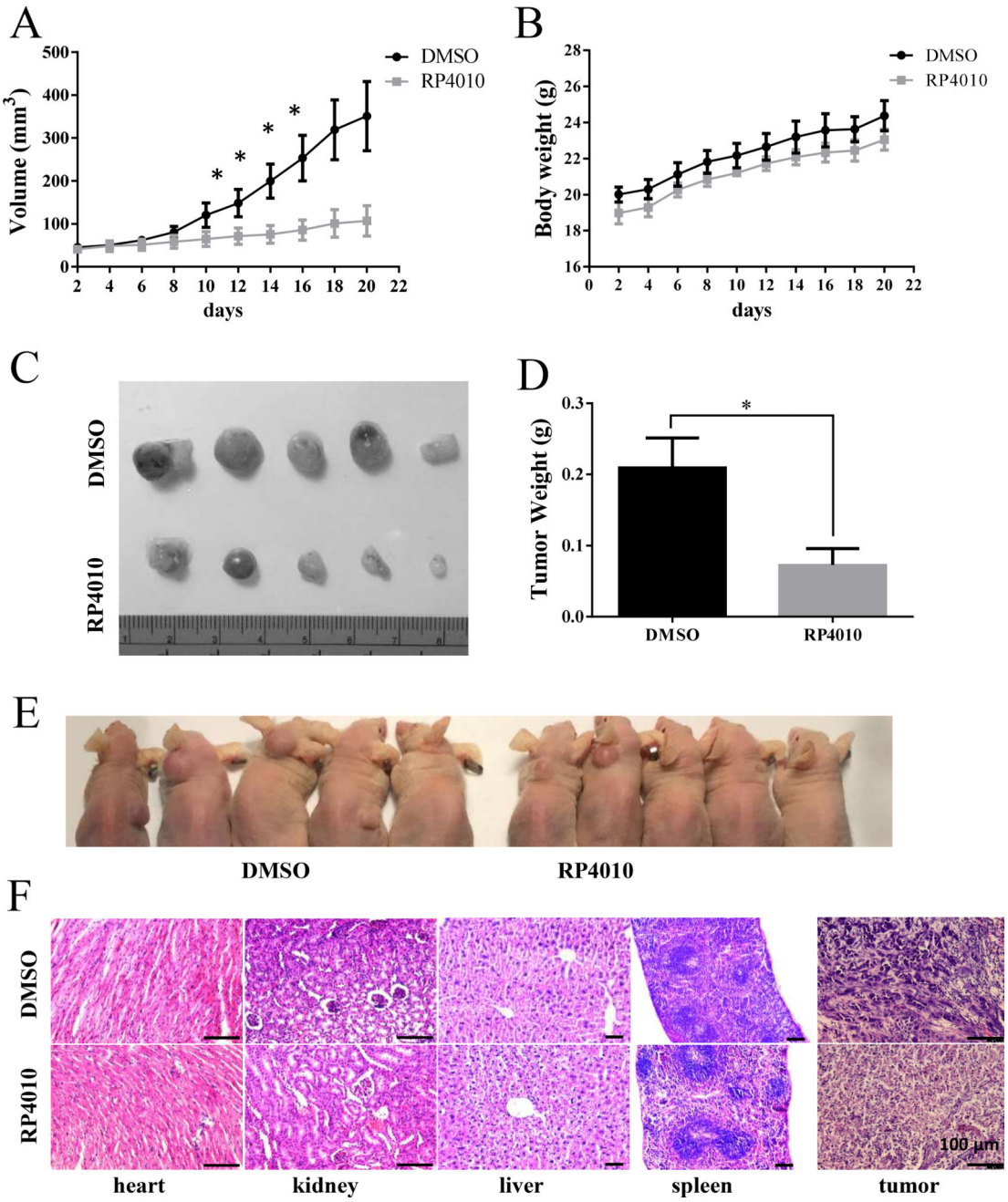

Figure 6.

RP4010 inhibited tumor growth in xenografted ESCC animals. (A) tumor volume growth curve. (B) changes in body weight. Nu/Nu mice were s.c. inoculated with 10^6 KYSE-150 cells and tumor became visible after 1 week. Then, vehicle control or RP4010 was I.P injected every other day for two weeks. (C) Image of xenograft tumor in RP4010 treatment and control groups. (D) The statistics of tumor weight in RP4010 treated and control groups. (E) H&E staining of heart, kidney, liver and spleen tissues. Scale bar, 100 μm.